ROBIN RAUL

NUMERICAL SOLUTION OF TURBULENT FLOWS

A new approach to turbulence modeling based on vorticity transport theory is described. A closed form of turbulent Navier–Stokes equations, which are derived by carrying out a Lagrangian analysis of the vorticity transport equation, is presented. To test the prediction capabilities of the model, two flow problems representing bluff body flows in two and three dimensions—around a square prism and around a cube—are simulated numerically using the model. Results are in good agreement with relevant experimental data.

INTRODUCTION

Most flows in nature are turbulent. Although they are governed by the laws of nature, flows pose a formidable mathematical problem. Because turbulence occurs in most flows of engineering and technological interest (around aircraft, automobiles, submarines, and tall structures, for example), it has interested scientists since the sixteenth century, when Leonardo da Vinci studied eddies in a stream. Science has since made much progress in the field of turbulence. Even though advances in experimental techniques have increased our understanding of turbulence phenomena, theoretical analyses and prediction methods have lagged.

This article surveys the difficulties in analyzing turbulence modeling and discusses state-of-the-art modeling techniques and solution methods. A new approach to turbulence modeling is described, and examples of its application are discussed. The article concludes with a look at future turbulence research.

REYNOLDS STRESSES

Flow of a Newtonian fluid, such as water or air, is described by Navier–Stokes equations that predict the balance of momentum acting on a fluid element because of various forces. In two dimensions with no external body forces, they are

x momentum,

$$\frac{\partial u}{\partial t} + u\frac{\partial u}{\partial x} + v\frac{\partial u}{\partial y} = -\frac{\partial p}{\partial x} + \frac{1}{Re}\left(\frac{\partial^2 u}{\partial x^2} + \frac{\partial^2 u}{\partial y^2}\right), \tag{1}$$

and y momentum,

$$\frac{\partial v}{\partial t} + u\frac{\partial v}{\partial x} + v\frac{\partial v}{\partial y} = -\frac{\partial p}{\partial y} + \frac{1}{Re}\left(\frac{\partial^2 v}{\partial x^2} + \frac{\partial^2 v}{\partial y^2}\right), \tag{2}$$

where u and v are velocities in x and y directions, respectively; t is time; p is pressure; and $Re = u_R l_R/\nu_l$ is the Reynolds number. Here, u_R is the reference velocity, l_R is a characteristic length, and ν_l is the kinematic viscosity. These equations and the continuity equation, which is a mathematical statement of the fact that the mass must be conserved and is written in two dimensions as

$$\frac{\partial u}{\partial x} + \frac{\partial v}{\partial y} = 0\,, \tag{3}$$

completely specify a fluid flow.

The goal of fluid dynamics is to seek a complete solution to the system of Equations 1, 2, and 3, subject to a given set of initial and boundary conditions. Difficulties arise because of the mathematical complexity of Navier–Stokes equations, which are inhomogeneous, nonlinear, coupled, partial differential equations. Their nonlinearity is responsible for the main difficulty in obtaining their solution. In turbulence calculations, nonlinearity introduces new terms in the equations, making the number of unknowns greater than the number of equations. This condition results in the so-called "closure problem," which is described in the following paragraphs.

The variables u, v, and p in Equations 1 and 2 are instantaneous values that consist of a mean and a fluctuating part. Hence, they can be decomposed in the following manner:

$$u = \bar{u} + u'\,,$$

$$v = \bar{v} + v'\,,$$

$$p = \bar{p} + p'\,, \tag{4}$$

where an overbar denotes the mean value and the prime denotes the fluctuating component. This is called Reynolds decomposition. Substitution of Equation 4 into Equations 1 and 2 and subsequent averaging yield

x momentum,

$$\frac{\partial \bar{u}}{\partial t} + \bar{u}\frac{\partial \bar{u}}{\partial x} + \bar{v}\frac{\partial \bar{u}}{\partial y} = -\frac{\partial \bar{p}}{\partial x} + \frac{1}{Re}\left(\frac{\partial^2 \bar{u}}{\partial x^2} + \frac{\partial^2 \bar{u}}{\partial y^2}\right) - \frac{\partial}{\partial x}(\overline{u'u'}) - \frac{\partial}{\partial y}(\overline{u'v'}) , \quad (5)$$

and y momentum,

$$\frac{\partial \bar{v}}{\partial t} + \bar{u}\frac{\partial \bar{v}}{\partial x} + \bar{v}\frac{\partial \bar{v}}{\partial y} = -\frac{\partial \bar{p}}{\partial y} + \frac{1}{Re}\left(\frac{\partial^2 \bar{v}}{\partial x^2} + \frac{\partial^2 \bar{v}}{\partial y^2}\right) - \frac{\partial}{\partial x}(\overline{u'v'}) - \frac{\partial}{\partial y}(\overline{v'v'}) . \quad (6)$$

In tensor notation, Equations 5 and 6 can be written jointly as

$$\frac{\partial \bar{u}_i}{\partial t} + \bar{u}_j\frac{\partial \bar{u}_i}{\partial x_j} = -\frac{\partial \bar{p}}{\partial x_i} + \frac{1}{Re}\frac{\partial^2 \bar{u}_i}{\partial x_j \partial x_j} - \frac{\partial}{\partial x_j}(\overline{u_i'u_j'}) . \quad (7)$$

The terms $\overline{u_i'u_j'}$, which are the correlations of the fluctuating velocities, are known as Reynolds stresses because their form is similar to viscous stresses. As mentioned earlier, Reynolds stresses result from the nonlinearity of the Navier–Stokes equations and represent the effect of turbulence on the mean flow field. Because no analytical form of the new terms is available, unknowns outnumber the equations; consequently, the system of equations is not closed, a problem that is at the heart of the difficulties in turbulence simulations.

EDDY VISCOSITY

Turbulence is accompanied by two major effects on the mean flow: diffusion (a great increase in the transport rate of mass, momentum, and energy) and dissipation (the conversion of kinetic energy into thermal energy). Since both phenomena are associated with viscosity in laminar flows, Boussinesq[1] postulated the following form of Reynolds stresses:

$$\overline{u_i'u_j'} = -\nu_t\left(\frac{\partial \bar{u}_i}{\partial x_j} + \frac{\partial \bar{u}_j}{\partial x_i}\right) + \frac{2}{3}k\delta_{ij} , \quad (8)$$

where ν_t is called eddy or turbulent viscosity and $k = \overline{u_i'u_j'}/2$ is turbulent kinetic energy. Unlike the laminar viscosity ν_l, which depends only on the given fluid, the eddy viscosity ν_t can depend on flow Reynolds number, flow geometry, buoyancy, and so on. To specify ν_t, Prandtl[2] proposed that, analogous to the laminar diffusion, the eddy viscosity must also be proportional to a turbulence length scale l and a turbulence velocity scale q; that is,

$$\nu_t = C_\mu q l , \quad (9)$$

where C_μ is either an empirical constant or a function of dimensionless parameters. Equation 9 is known as the "mixing length theory," and l is known as the "mixing length." To use the mixing-length hypothesis in computations, it is necessary to specify the turbulence scales l and q.

TWO-EQUATION MODELS

In earlier mixing-length models, q and l were specified as algebraic functions of the mean variables. These so-called "algebraic eddy viscosity models" are not sufficiently accurate for nonsimple flows, that is, flows with strong shear, separation, reattachment, recirculation, and so on. One reason for this inadequacy is that the mixing-length concept is based on local equilibrium; that is, it assumes that the production and dissipation of the turbulent kinetic energy at each point in the flow are equal. Thus, the concept ignores the effects of turbulence transport and history.

To overcome this drawback, Jones and Launder[3] proposed that q and l should be obtained dynamically at every point in the flow. In this "two-equation model," or k–ϵ model, the turbulence velocity scale $q = \sqrt{k}$ is obtained by

$$\underbrace{\frac{\partial k}{\partial t} + \bar{u}_i\frac{\partial k}{\partial x_i}}_{\{1\}} = \underbrace{-\overline{u_i'u_j'}\left(\frac{\partial \bar{u}_i}{\partial x_j} + \frac{\partial \bar{u}_j}{\partial x_i}\right)}_{\{2\}} \underbrace{- \nu_l\frac{\overline{\partial u_i'\partial u_i'}}{\partial x_j \partial x_j}}_{\{3\}} + \underbrace{\frac{\partial}{\partial x_i}\left(\frac{\nu_t}{\sigma_k}\frac{\partial k}{\partial x_i}\right)}_{\{4\}} . \quad (10)$$

The transport equation for k is the mathematical statement of the fact that the rate of change of turbulent kinetic energy is influenced by convective transport by mean motion (term {1}), production by mean velocity gradients (term {2}), dissipation by viscosity (term {3}), and diffusion by turbulent motion (term {4}). Equation 10 is derived from Navier–Stokes equations except for term {4}, which has been added on the assumption that the diffusion of k is proportional to the gradient of k. Here σ_k is an empirical constant.

Since the turbulence length scale (the length over which dissipation occurs) is directly related to the turbulent energy equation, an expression relating the two quantities is required. Assuming that the dissipation rate ϵ is governed by turbulent motion characterized by ve-

locity scale $\sqrt{k}$ and length scale l, a dimensional analysis leads to

$$\epsilon \propto \frac{k^{3/2}}{l} \quad . \tag{11}$$

Using Equations 11 and 9, the expression for the turbulent viscosity becomes

$$\nu_t = C_\mu \frac{k^2}{\epsilon} \quad , \tag{12}$$

where the constant of proportionality has been absorbed in C_μ. Although an exact equation for ϵ can be derived from Navier–Stokes equations, and, to reduce it to a computable form, assumptions of a highly empirical nature are required, the dissipation rate equation is usually written as

$$\underbrace{\frac{\partial \epsilon}{\partial t} + \bar{u}_i \frac{\partial \epsilon}{\partial x_i}}_{\{1\}} = \underbrace{C_1 \frac{P\epsilon}{k}}_{\{2\}} - \underbrace{C_2 \frac{\epsilon^2}{k}}_{\{3\}} + \underbrace{\frac{\partial}{\partial x_i}\left(\frac{\nu_t}{\sigma_\epsilon}\frac{\partial \epsilon}{\partial x_i}\right)}_{\{4\}}, \tag{13}$$

where

$$P = -\overline{u_i' u_j'}\left(\frac{\partial \bar{u}_i}{\partial x_j} + \frac{\partial \bar{u}_j}{\partial x_i}\right) \quad ;$$

$$\epsilon = \nu_1 \overline{\frac{\partial u_i'}{\partial x_j}\frac{\partial u_i'}{\partial x_j}}$$

is the dissipation rate; and C_1, C_2, and σ_ϵ are model constants. Here the terms {1} through {4} represent the physical processes governing the rate of dissipation, transport by convection and diffusion, and production and dissipation, respectively. As can be seen from the preceding equations, the two-equation model requires five inputs: C_μ, σ_k, σ_ϵ, C_1, and C_2. These constants are determined from either experiments or from numerical calculations.

The two-equation model contains many shortcomings. For instance, the standard form of the model is applicable only to high Reynolds number flows. Its performance is poor in low Reynolds number flows and regions close to a solid wall (where viscous effects dominate). Another fundamental deficiency of the k–ϵ model occurs with the use of the mixing-length concept. Inherent in the mixing-length theory is the assumption that the pressure does not affect the transport of momentum, which is clearly unphysical. Many modifications have been proposed to overcome these difficulties. Excellent reviews are given by Ferziger,[4] Lakshminarayana,[5] and Lumley.[6] Despite its drawbacks, the k–ϵ model is widely used in most engineering applications for two reasons: no better prediction models requiring equivalent effort exist, and the model still provides results of engineering accuracy for simple flows.

HIGHER–ORDER MODELS AND CHAOS

Higher-order turbulence models, such as the Reynolds stress model used to solve equations for each of the Reynolds stresses, require considerably greater computer resources. Large eddy simulations are another class of models through which only the small-scale eddy motions are modeled and large eddies (coherent structures) are computed. The era of supercomputers has resulted in direct numerical simulations in which all scales of turbulence are resolved on an extremely fine mesh that contains several million grid points.

Inspired by the success of the theory of chaos in other nonlinear dynamic systems, fluid dynamists have recently proposed using the same theory for simulating turbulence statistics. Turbulence, which is governed by nonlinear dynamical equations and exhibits coherent structures, seems particularly well-suited to the tools of the chaos theory. Some attempts are the study of the strange attractor theory of turbulence,[7] the prediction of chaos for infinite dimensional dynamic systems,[8] and the use of fractals in fluid mechanics.[9]

VORTICITY TRANSPORT THEORY

In 1915, G. I. Taylor proposed an alternative approach[10] to turbulence modeling. He argued that vorticity, which is twice the angular momentum of a fluid element, and not linear momentum, is conserved in a two-dimensional flow; hence, vorticity should be taken as the transferable quantity instead of momentum. He showed that vorticity transport theory is consistent with the physics and gives accurate predictions. Later he extended his theory to three dimensions,[11] but, since vorticity is not conserved in three dimensions, he had to make several restrictive assumptions. The theory's final form, known as the modified vorticity transport theory, was impractical in a computational sense. Consequently, vorticity transport theory remained in the background.

Because vorticity dynamics play a major role in the development of a fluid flow, many theoretical and experimental investigations of vortical structures in turbulent flows have been made. The discovery of coherent structures in turbulent boundary layers has further intensified these efforts. Since Chorin[12] showed that a workable transport model can be obtained using a coarse graining hypothesis, renewed interest in vorticity gradient law has resulted. The vorticity theory has been further developed by Bernard[13] and Bernard and Berger[14] using a precise mathematical framework. Their scheme relies on a Lagrangian analysis of the transport correlations that were anticipated by Taylor but never completed. The resulting three-dimensional closure model is called the mean vorticity and covariance (MVC) closure, a brief description of which is given in the following paragraphs.

Equation 7 can be transformed into the vorticity transport form using the identity

$$\frac{\partial}{\partial x_j}\left(\overline{u_i' u_j'}\right) = -\epsilon_{ijk}\overline{u_j' \omega_k'} + \frac{\partial}{\partial x_i}\left(\frac{\overline{u_j' u_j'}}{2}\right) \quad , \tag{14}$$

where ϵ_{ijk} is the alternating tensor and ω_k''s are the fluctuating vorticity components. Substituting Equation 14 into Equation 7 and replacing $\overline{u_j' u_j'}/2$ by k, Equation 7 becomes

$$\frac{\partial \bar{u}_i}{\partial t} + \bar{u}_j \frac{\partial \bar{u}_i}{\partial x_j} = -\frac{\partial}{\partial x_i}(\bar{p} + k) + \frac{1}{Re}\frac{\partial^2 \bar{u}_i}{\partial x_j \partial x_j} + \epsilon_{ijk}\overline{u_j' \omega_k'} . \quad (15)$$

This operation has converted the unclosed term containing the transport of linear momentum by turbulent fluctuations to another unclosed term containing the transport of vorticity. The MVC closure is thus used to obtain closed relations for the last term in Equation 15, which is achieved by integrating the exact vorticity equation along a particle path, forming the product $\overline{u_j' \omega_k'}$, and analyzing each term in the ensuing expression. After making several appropriate assumptions,[15] the following approximation is obtained:

$$\overline{u_j' \omega_k'} = -\overline{u_j' u_n'} T \bar{\omega}_{k,n} + Q\overline{u_j' u_{k,n}' \omega_n} , \quad (16)$$

where T and Q are Lagrangian integral time scales. The second term on the right side represents the nongradient contribution to the correlation $\overline{u_j' \omega_k'}$. This expression is used to close the momentum equation (Eq. 15), and the vorticity transport equation is obtained by taking the curl of the closed momentum equation.

TWO–DIMENSIONAL MVC CLOSURE

In its most general form, the vorticity transport closure scheme used in computing two-dimensional flows requires the solution of dynamical equations for the vorticity mean $\bar{\omega}_3$ and four components ζ_{11}, ζ_{22}, ζ_{33}, and ζ_{12} of the vorticity covariance $\zeta_{ij} \equiv \overline{\omega_i' \omega_j'}$. If the flow is two-dimensional in the mean, $\bar{\omega}_1 = \bar{\omega}_2 = 0$ and $\zeta_{23} = \zeta_{13} = 0$. In the following discussion, the notation $\bar{\omega} = \bar{\omega}_3$ will be used. Coupled to these equations are kinematic relations from which the mean velocity field $(\bar{u}_1, \bar{u}_2)$ is determined from $\bar{\omega}$ and the Reynolds stresses $\overline{u_1'^2}$, $\overline{u_2'^2}$, $\overline{u_3'^2}$, and $\overline{u_1' u_2'}$ are obtained from ζ_{ij}. The mean velocity components can be determined from a mean stream function $\bar{\psi}$ by the relations

$$\bar{u}_1 = \frac{\partial \bar{\psi}}{\partial x_2} \quad (17)$$

and

$$\bar{u}_2 = -\frac{\partial \bar{\psi}}{\partial x_1} , \quad (18)$$

once the Poisson equation,

$$\nabla^2 \bar{\psi} = -\bar{\omega} , \quad (19)$$

is solved for $\bar{\psi}$.

Because of the extensive computational requirements entailed in solving for a complex nonsteady flow field, just the trace $\zeta \equiv \zeta_{ii}$ of ζ_{ij} is solved instead of separate equations for each of the four separate components of ζ_{ij}. Consequently, the kinematic problem of calculating $\overline{u_i' u_j'}$ from ζ_{ij} is reduced to one of computing only the turbulent kinetic energy k from ζ.

After some approximations warranted by the replacement of ζ_{ij} by ζ, it follows that the dynamical equations for $\bar{\omega}$ and ζ in two dimensions are, respectively,

$$\frac{\partial \bar{\omega}}{\partial t} = -\bar{u}_j \frac{\partial \bar{\omega}}{\partial x_j} + \frac{\partial}{\partial x_j}\left\{\left(\nu_1 + \frac{2}{3} kT\right)\frac{\partial \bar{\omega}}{\partial x_j}\right\} + \frac{\partial}{\partial x_j}\left(\frac{\frac{2}{3} Q_1 \bar{\omega} \frac{\partial k}{\partial x_j}}{1 + Q_1 Q_2 \bar{\omega}^2}\right) \quad (20)$$

and

$$\frac{\partial \zeta}{\partial t} = -\bar{u}_j \frac{\partial \zeta}{\partial x_j} + \frac{\partial}{\partial x_j}\left\{\left(\nu_1 + \frac{2}{3} kT\right)\frac{\partial \zeta}{\partial x_j}\right\} + \frac{4}{3} kT \frac{\partial \bar{\omega}}{\partial x_j}\frac{\partial \bar{\omega}}{\partial x_j} + 2S\bar{\omega}^2 \Gamma_1 + 2S\zeta\Gamma_1 + 4S\Gamma_1\Gamma_2 - \frac{14\nu\zeta}{\lambda^2} , \quad (21)$$

where the summation is for $j = 1, 2$. Here, T, S, Q_1, and Q_2 are Lagrangian integral time scales, $\Gamma_1 = 4k/\lambda^2$, $\Gamma_2 = (\zeta - 3\Gamma_1)/2$, and λ is a microscale, which is a measure of the smallest eddies present in a given flow. These eddies are mainly responsible for the dissipation and hence are sometimes referred to as dissipation scale. The first and second terms on the right sides of Equations 20 and 21 represent advection and diffusion processes, respectively. The total diffusivity in each equation is given by $\nu_1 + 2/3kT$, which reflects a viscous and turbulent contribution. The last two terms in Equation 20 account for vortex stretching and shearing phenomena. Turbulence production arising from the mean flow is accounted for in the ζ equation by the third and fourth terms on the right side. The second and the third-to-last terms in Equation 21 represent turbulence self-production effects, and the final term expresses dissipation. (A discussion of the derivation of Equations 20 and 21 can be found in Ref. 16.) The last term in Equation 20 results from the nongradient term of the closure relation, Equation 16, and was neglected in the previous applications of the closure. But since it has been shown that nongradient contributions can be of considerable importance,[17] they were included in the present applications.

A general kinematic relationship between ζ and k is

$$\zeta = \frac{12k}{\lambda^2} + \frac{1}{2k}\nabla k \cdot \nabla k \quad (22)$$

and is derived as a simplification of the defining equations for the microscales associated with the two-point Eulerian velocity correlation coefficient. Using the quantities Γ_1 and Γ_2 defined previously, Equation 22 can be expressed as $\zeta = 3\Gamma_1 + 2\Gamma_2$.

Equations 21 and 22 make it evident that an additional relation from which λ can be computed is needed in the present approach. The relation can be developed from a family of solutions for the decay of isotropic turbulence that was first described by Sedov.[18] One part of the result is the microscale equation

$$\frac{d\lambda}{dt} = -\frac{\delta}{2}\sqrt{\zeta}\,\lambda + \frac{2\nu_1}{\lambda} , \tag{23}$$

where δ is a constant proportional to the skewness factor of the velocity derivative fluctuations. This relation governs the variation of λ in time from the initial state. The first term on the right side reduces λ by vortex stretching, and the second is responsible for an increase in λ because of viscous diffusion. During the isotropic decay process, λ will change in time. In flows containing a source of turbulence because of a mean shear, however, it may be hypothesized that the opposing processes of vortex stretching and viscous diffusion will be in balance and that this equilibrium will be maintained at all times in the face of changes in the mean flow field. It follows that $d\lambda/dt \approx 0$ and, consequently, that

$$\lambda^2 = \frac{4\nu_1}{\delta\sqrt{\zeta}} . \tag{24}$$

For this study, the time scales T, Q_1, Q_2, and S were computed as in earlier applications.[19,20] In particular, T, Q_1, and Q_2 were set to constants, whereas the scale S was given by

$$S = \frac{C_S k}{\nu_1 \zeta^*} , \tag{25}$$

where C_S is a constant and $\zeta^* \equiv 12k/\lambda^2$, an expression suggested by dimensional arguments.[21] An attractive feature of Equation 25 is that with it the stability of the ζ equation can be virtually guaranteed, since the turbulent self-production term in Equation 21 can be arranged to be always bounded by the dissipation term. To see this, note that Equations 22, 24, and 25 imply that

$$2S\zeta\Gamma_1 + 4S\Gamma_1\Gamma_2 - \frac{14\nu\zeta}{\lambda^2} \le 0 ,$$

if

$$2S\zeta^2 - \frac{14\nu\zeta}{\lambda^2} = -\zeta^{3/2}\left(\frac{7}{2}\,\delta - \frac{2}{9}\frac{C_S}{\delta}\right) \le 0 .$$

Thus, finite solutions to Equation 21 should exist as long as

$$\frac{7}{2}\,\delta - \frac{2}{9}\frac{C_S}{\delta} > 0 . \tag{26}$$

This relation acts as a constraint on the selection of C_S and δ that must always be satisfied.

To summarize, the complete set of equations to be solved consists of dynamical Equations 20 and 21 for $\bar{\omega}$ and ζ, respectively, and kinematic Equation 19 for $\bar{\psi}$ and Equation 22 for k. Finally, λ^2 is given by Equation 24 and S by Equation 25. The externally supplied quantities to the system of equations consist of the five constants, T, Q_1, Q_2, C_S, and δ.

TEST PROBLEMS

The ultimate test of any theory is its ability to predict accurately problems of practical importance. Here, two-dimensional unsteady flow around a square prism and three-dimensional flow around a cube are chosen as test problems for several reasons:

1. They are representative of bluff body flows in two and three dimensions, respectively. Such flow phenomena are associated with many technologically important flows, such as those around aircraft fuselages, submarines, automobiles, and tall structures.

2. They contain sufficiently complex flow phenomena such as separation, recirculation, reattachment, and vortex shedding, and make stringent test cases for testing turbulence models.

3. Their simple geometry allows the use of a Cartesian grid, freeing up computer space for other things such as finer grid resolution.

In the next section, numerical schemes used to solve the two test problems are discussed, followed by results of the computations and conclusions.

NUMERICAL SCHEME

The governing equations, given here for the two-dimensional flow and given elsewhere[16] for the three-dimensional flow, were solved numerically. The computational mesh used for the square flow and cube flow is shown in Figures 1 and 2, respectively. For the cube flow, it is necessary only to solve in the quarter domain because the flow is symmetric about the y and z axes. Consequently, Figure 2 shows only the quarter domain of the cube flow field.

The spatial derivatives were approximated using second-order central differences, and first-order backward differences were used for the time derivatives. The discrete equations were solved iteratively using a semi-implicit successive-over-relaxation scheme in which the computational space is swept in a systematic manner and every alternate point is updated during each pass. Such a technique is well-suited for vector computers, and significant improvements in speed can be achieved.

The general procedure to advance the solution in time is the same for both test cases, except that, for the cube,

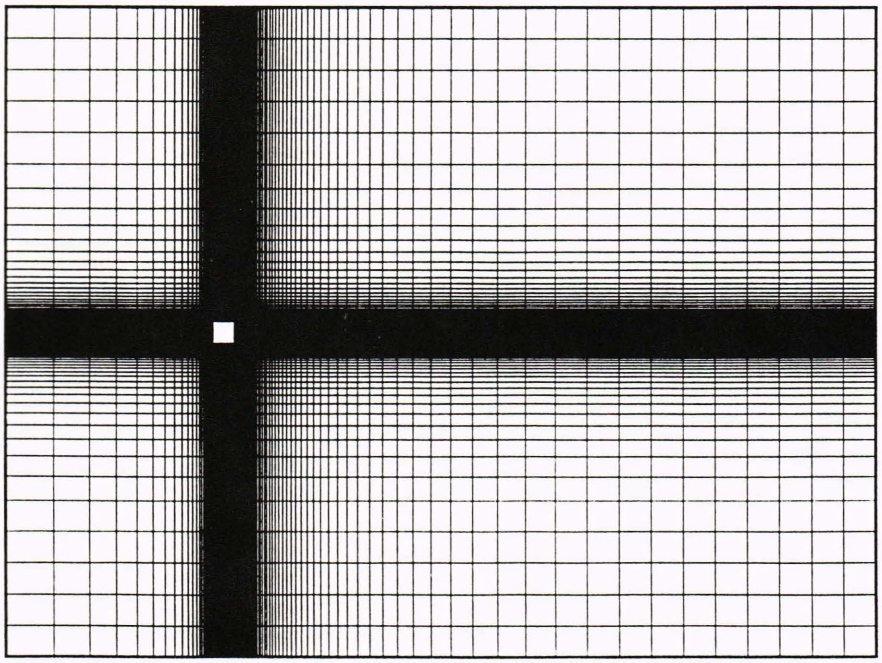

Figure 1. Computational grid, square flow.

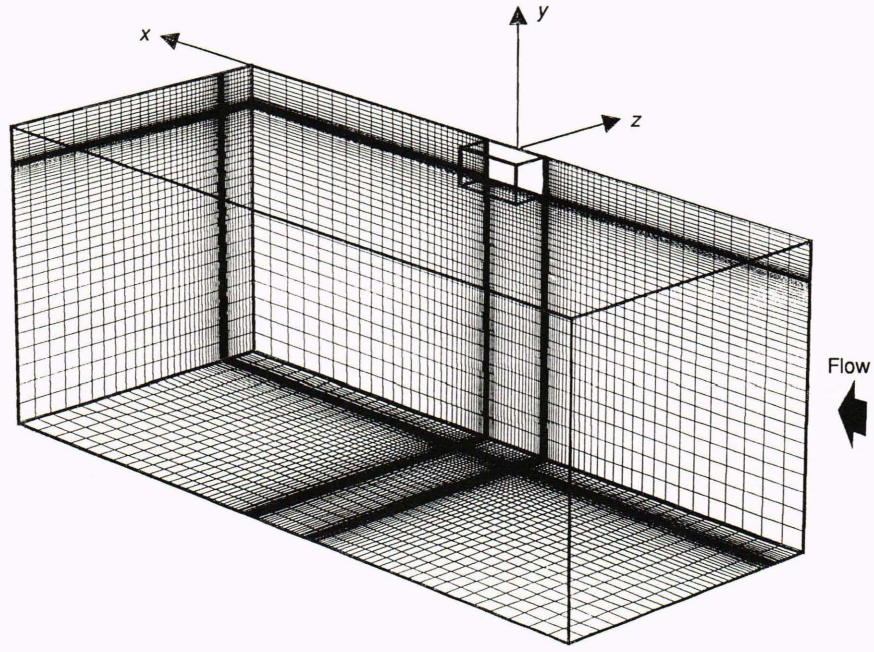

Figure 2. Computational grid, cube flow.

the stream function is replaced by its three-dimensional analog—namely, the vector potential. A typical solution cycle consists of the following steps:

1. The mean vorticity $\overline{\omega}$ is advanced in time by solving Equation 20.

2. The mean stream function $\overline{\psi}$ (the vector potential in three dimensions) is then updated by solving the Poisson equation (Eq. 19).

3. With the new $\overline{\psi}$ field, the velocity components and hence the vorticity on the boundaries are obtained using their definitions.

4. The covariance field ζ is next calculated using Equation 21.

5. Finally, the turbulent kinetic energy k corresponding to the new covariance field is obtained from the kinematic equation (Eq. 22), and the cycle is repeated.

NUMERICAL RESULTS

Square Flow

The calculations were performed at $Re = 2000$ using a mesh with 120 by 100 grid points in the x and y directions, respectively. The computational domain, shown in Figure 1, extended from −10 to +20 in the x direction and −10 to +10 in the y direction, where the square has sides of unit length. The time step was $\Delta t = 0.001$, and the

constants used in the turbulence model were set to T = 0.3, C_S = 0.07, δ = 0.037, Q_1 = 0.1, and Q_2 = 0.01.

Figure 3 shows the variation of drag and lift during several cycles of the computed flow field. The drag, as expected, fluctuates at twice the shedding frequency. The average drag coefficient, $C_{D_{ave}} = 2D/(\rho u_\infty^2 h)$, where D is drag, ρ is the fluid density, u_∞ is free-stream velocity, and h is the exposed area, was 2.05, and the lift coefficient varied between ±0.39. The average drag compares well with the experimental results of Lee,[22] who found $C_{D_{ave}}$ = 2.05 at Re = 176,000, and of Nakaguchi et al.,[23] who measured $C_{D_{ave}}$ = 2.05 at $Re = 0(10^4)$. It is also relatively close to the values reported by Bearman and Trueman,[24] who found $C_{D_{ave}}$ = 2.2 for Re in the range from 20,000 to 70,000. The computed peak lift is considerably less than the measured rms value of 1.31 at $Re = 0(10^5)$ reported by Vickery,[25] or the peak lift of 1.4 for Re between 33,000 and 130,000 given by Nakamura and Mizota.[26] The discrepancy may be a Reynolds number effect because the current value of 2000 is much less than that used in previous experiments. The predicted lift could be severely affected by the proximity of the outer boundary as well as by the coarseness of the mesh used in the far field in the lateral direction. Such effects are of great importance, particularly in two-dimensional calculations.

Figure 4 shows the variation of $\bar{v}$ at two locations on the axis behind the square. It was observed that the maximum magnitude of the transverse velocity is about 0.82. Further, no subharmonics were discerned in the present calculations as was also true in experimental observations. On the basis of variations of lift, drag, and transverse velocity, the average Strouhal number $St = fa/u_\infty$, where f is the shedding frequency, a is the square side, and u_∞ is the free-stream velocity, was calculated to be 0.147. This value is a little higher than the experimental value of 0.135 at Re = 2000 reported by Davis and Moore.[27] Some significant scatter occurs in the data presented for St. For example, the lowest value of St is reported as 0.12 by Vickery,[25] and the highest is 0.138 given by Durao et al.[28] Experiments show that the square cylinder flow does not become Re-independent until after Re = 10,000, when St achieves a constant value of 0.13.[29]

Figure 5 shows the instantaneous streamlines (left column) and the associated vorticity fields (right column) at several instants during one shedding cycle. The sequence shows how vorticity created at the leading sharp corners is alternately shed downstream. In Figure 6, the streamlines averaged over several cycles are shown. Comparison of this figure with the results of Durao et al.[28] reveals that the present prediction for wake size at Re = 2000 is slightly larger than that at Re = 14,000, although the qualitative agreement is good. A similar conclusion can be drawn from the distribution of average axial velocity along the streamwise axis of the square. Figure 7 shows the experimental results of Durao et al.[28] at Re = 14,000 compared with the present solution and the numerical results of Durao et al.[30] using the k–ϵ turbulence model to solve for the square flow at Re = 14,000. In the latter calculation, the coefficients in the k–ϵ model were adjusted to obtain an accurate prediction

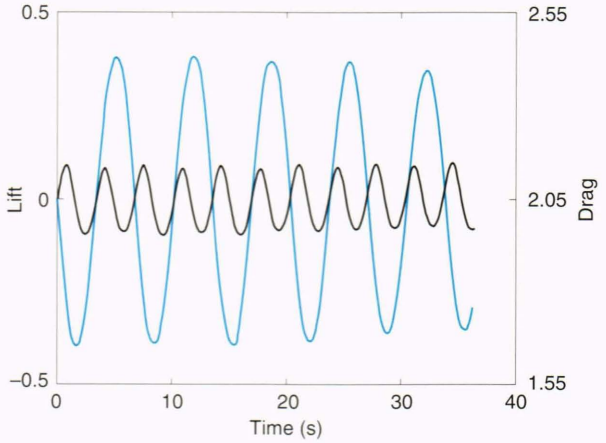

Figure 3. Variation of drag and lift with time. Black line = drag. Blue line = lift.

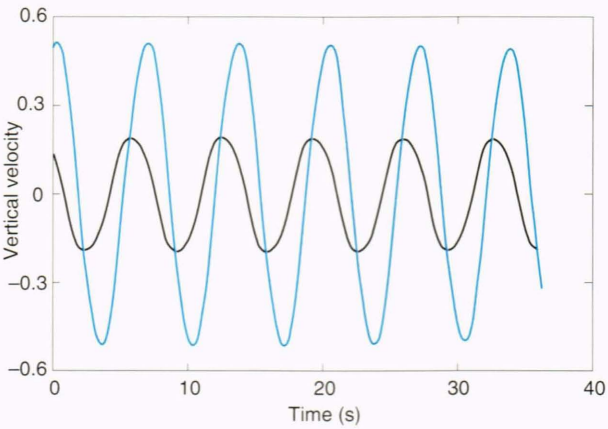

Figure 4. Vertical velocity in wake. Black line: x_1 = 0.52. Blue line: x_1 = 1.01.

of the size of the recirculation bubble. As is evident from Figure 7, however, the magnitude of $\bar{u}$ was underpredicted, and, in fact, no separation was found to occur on the sides of the square. These deficiencies can be attributed to the fact that the k–ϵ model is unable to account for the anisotropy, history, and transport effects in a complex flow such as the present one.

Cube Flow

The cube calculations were performed at Reynolds numbers of 2000 and 14,000 on the computational mesh shown in Figure 2. As mentioned earlier, the computations were done on the quarter domain. The origin of the coordinate system is set at the cube center. All lengths are nondimensionalized with the cube dimension so that the cube is of dimension unity, and the finite-difference mesh extends from –5 to +5 in the x direction and – 4 to 0 in the two lateral directions. The computational mesh was designed to provide maximum resolution near the cube surfaces.

The values of the constants appearing in the turbulence equations were set to δ = 0.037, C_S = 0.007, T = 0.25, Q_1 = 0.1, and Q_2 = 0.01 for the computations at Re = 2000, and to δ = 0.01, C_S = 0.001, T = 0.25, Q_1 = 0.1,

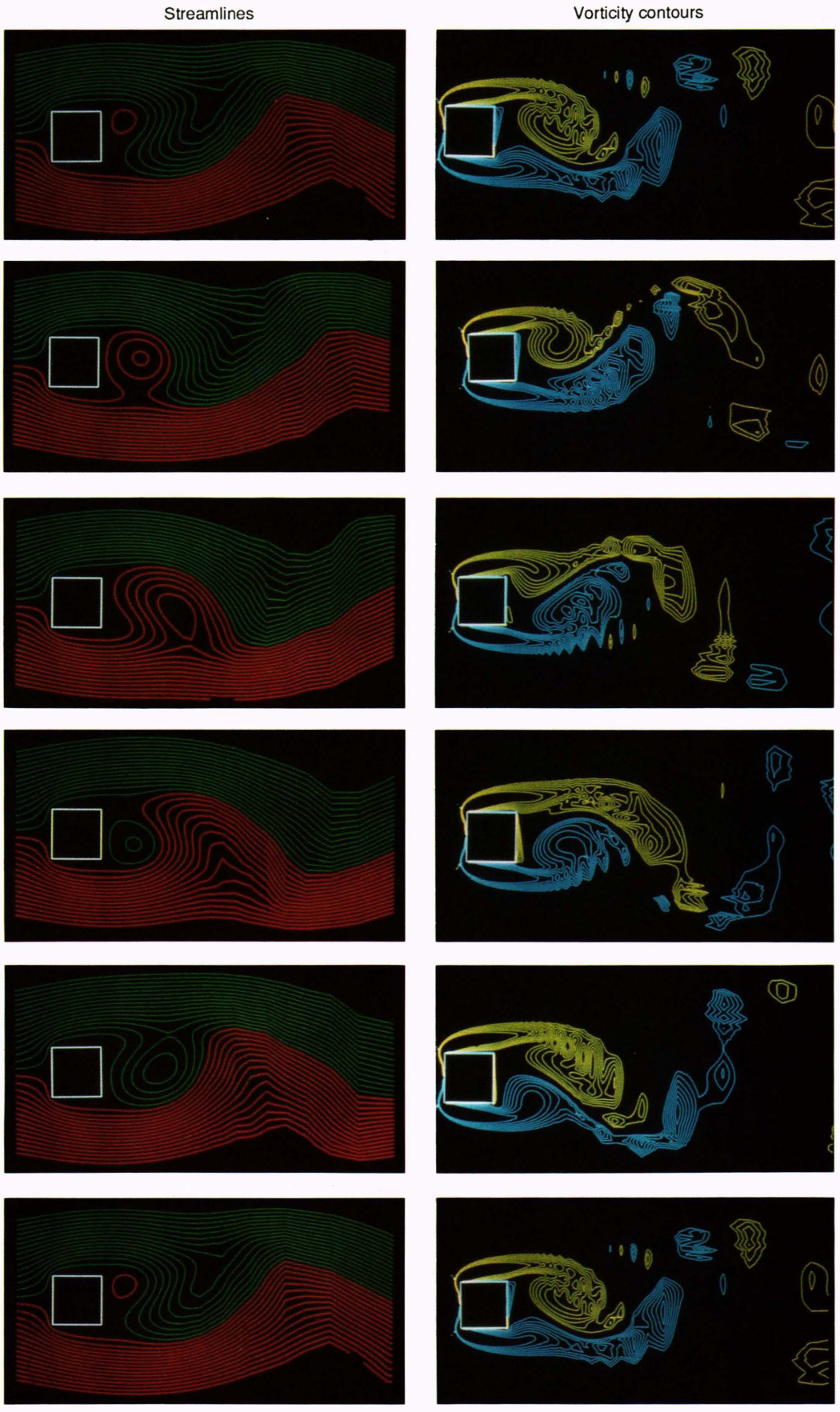

Figure 5. Streamlines (left) and vorticity contours (right) at various stages during one shedding cycle.

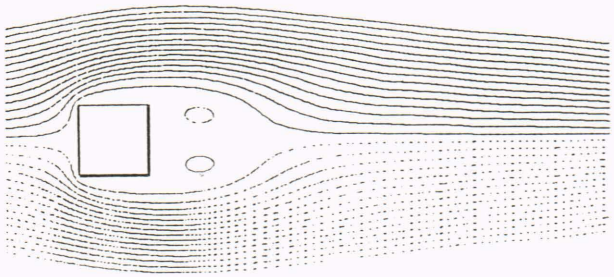

Figure 6. Streamlines averaged over several cycles.

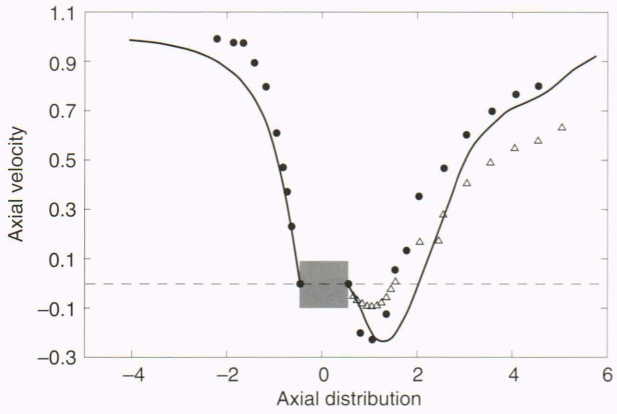

Figure 7. Averaged $\bar{u}_1$ velocity on the square axis. Solid line: present results. Solid circle: experiments by Durao et al.[28] Open triangle: k–ϵ model calculation by Durao et al.[30]

and $Q_2 = 0.01$ at $Re = 14{,}000$. The selection of the values was based on previous studies of channel and jet flow fields in which allowance was made for the differing Reynolds numbers.

The drag coefficient calculated at $Re = 2000$ reached a steady-state value of 1.23, whereas at $Re = 14{,}000$ it was 1.17. These values are compared with experimental data in Figure 8, including a result of Nakaguchi's,[31] who measured drag coefficients of bars of square cross section aligned with the flow. Extrapolation of the results gives C_D for a cube as 1.17 for $Re = 1.7 \times 10^5$. Nakaguchi also reported that the drag value did not show any appreciable change for Re between 0.77×10^5 and 2.3×10^5. An additional data point is given by Anderson,[32] who reported a value of $C_D = 1.09$ for the cube flow at $Re = 3 \times 10^5$. To further display what is to be expected at other Reynolds numbers, the drag caused by a square flat plate held normal to the flow[33] is also shown in Figure 8 as well as some results for laminar flows reported earlier.[34]

The character of the computed flow field can be deduced from the series of velocity vector plots contained in Figures 9 to 11 for the $Re = 2000$ solution. The flow at $Re = 14{,}000$ shows many of the same features. A view of the cube flow in the x–y plane through its midpoint is shown in Figure 9. The wake is much longer here as compared with the laminar case.[34] In contrast to the laminar solution, a region of reverse flow occurs that extends about halfway along the sides of the cube. Flow separation begins a little aft of the front edge and not exactly at it, as has been observed in earlier studies of two-dimensional bluff body flows.[35,36] Along the side surfaces of the cube, a zone of relatively stationary fluid exists. The general attributes of the computed flow field agree with experimental observations by Anderson[32] at $Re = 3 \times 10^5$, who observed that dye placed on the side surfaces of the cube did not show significant motion.

A three-dimensional view of the complete separation zone containing velocity vectors just off the surface is shown in Figure 10. The view is from the rear of the cube and shows that flow reversal reaches a maximum along the central point of the sides, whereas none occurs near the edges. An interesting vortical circulation pattern is also evident as the flow negotiates past the front corners. Near the rear edges of the cube the flow is away from the corners.

Figure 11 is a view of the wake of the cube at $x = 0.64$. The flow here is toward the cube to fill in the wake. The motion on the rear face is toward the edges as a manifestation of the presence of counter-rotating vortical pairs formed around each corner. This motion accounts for the influx of high-speed fluid toward the center of the rear edges of the cube.

Experimental or numerical predictions of turbulence levels in the cube flow with which the present results may be compared appear to be unavailable. Nonetheless, to give some idea of the turbulent field computed in the present example, contours of ζ in the central plane $z = 0$

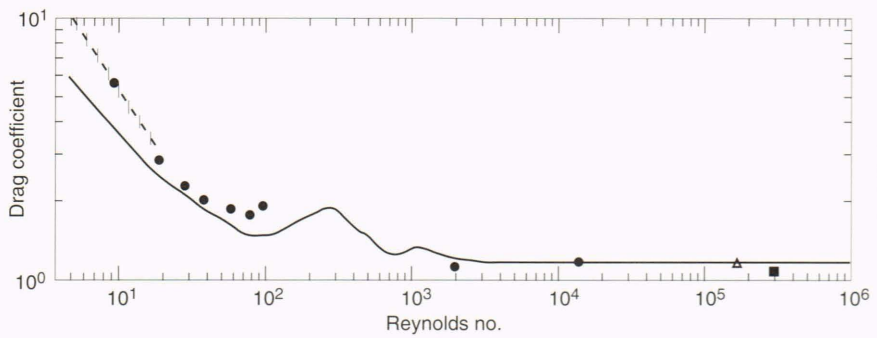

Figure 8. Drag versus Reynolds number. Solid circles: present calculations. Open triangle: Nakaguchi[31] data. Solid square: Anderson[32] data. Solid line: flat plates normal to the flow. Dashed line: experiments by Raul.[16]

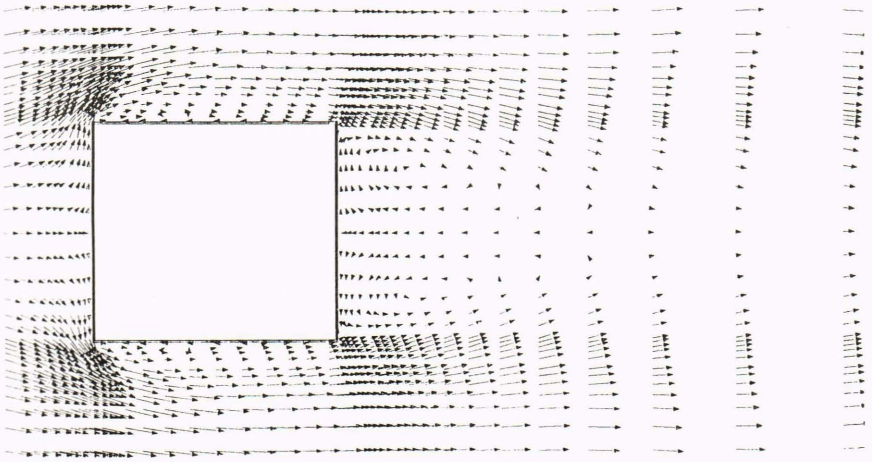

Figure 9. Velocity vectors on $z = 0.0$ plane at a Reynolds number of 2000.

are shown in Figure 12. Extremely high levels of turbulence are evident along the front edge of the cube, with the greatest concentration at the sharp corner. Since the turbulence produced here is unable to convect or diffuse very far upstream of the cube, a relatively sharp interface between the turbulence and upstream potential regions of the flow is evident. The turbulence generated at the front face convects outward and downstream, forming a decaying turbulent wake. Some additional turbulence is generated as the fluid passes the rear edge of the cube.

Further insight into the computed turbulent field may be obtained from Figure 13, which shows profiles of the scaled turbulent kinetic energy k/u_∞^2 for the $Re = 14{,}000$ solution at several stations along and behind the cube. The highest level of k occurs just off the front edge of the cube on the line that is flush with the front face. The region of significant turbulent activity broadens outward along the sides of the cube and into the wake. A slight narrowing of the wake can also be observed as well as the convection and diffusion of turbulence into the region directly behind the cube. Turbulence generated at the rear edge of the cube is responsible for the secondary peak in k at this location.

Finally, to reveal the structure of the cube wake, some particle traces were made. They were obtained by introducing massless particles in the wake and then following their time evolution. One such trace is shown in Figure 14, where the motions of three particles introduced in the wake are plotted. The particles introduced in the center plane and in a diagonal plane remain in their respective planes. A third particle introduced just above the center plane moves toward the nearest diagonal plane in a spiral motion.

CONCLUSIONS

A vorticity-based turbulence closure model has been derived using Lagrangian analysis of the vorticity trans-

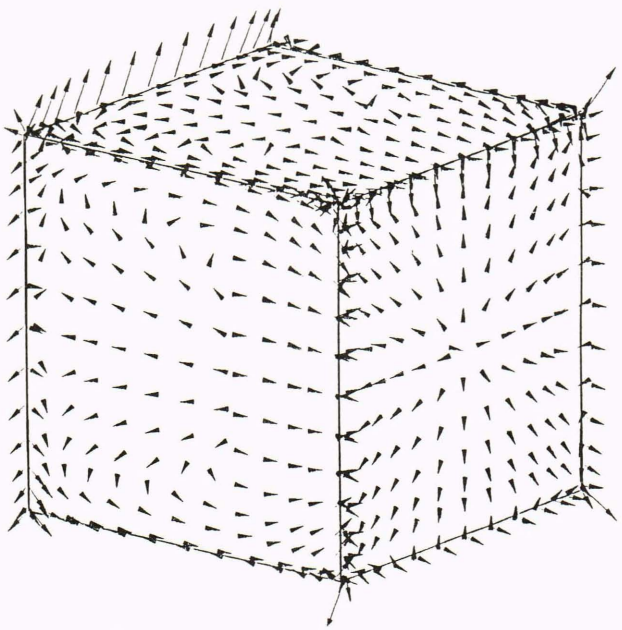

Figure 10. Velocity vectors just off the cube surface at a Reynolds number of 2000; three-dimensional view from rear.

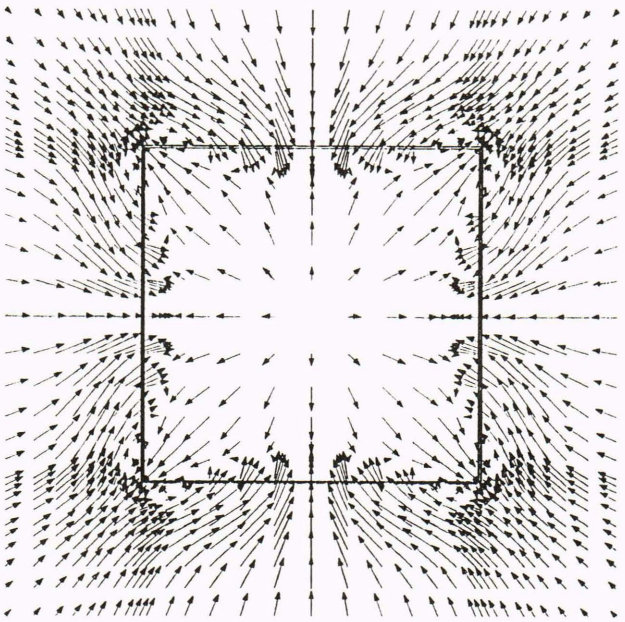

Figure 11. Velocity vectors on $x = 0.64$ plane at a Reynolds number of 2000.

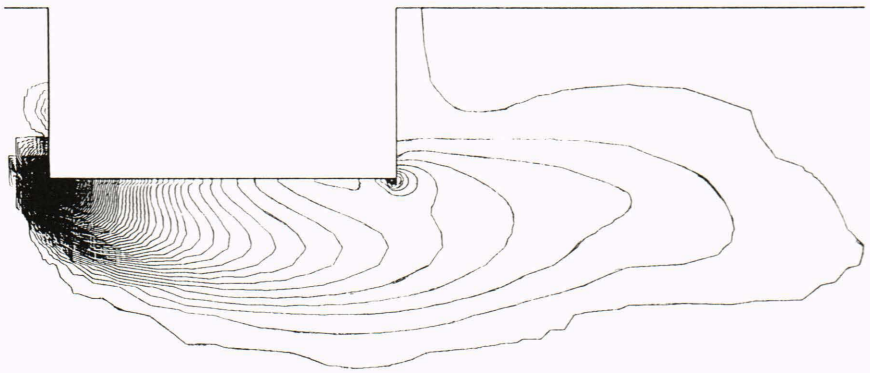

Figure 12. Contours of the vorticity covariance ζ on $z = 0.0$ plane at a Reynolds number of 2000.

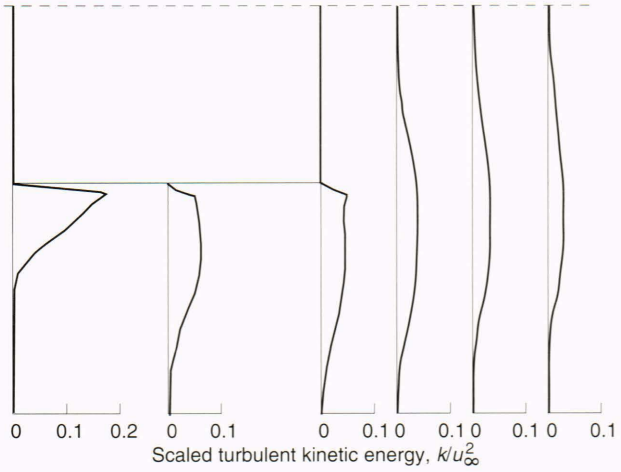

Figure 13. Cross sections of scaled turbulent kinetic energy k/u_∞^2 at a Reynolds number of 14,000 at several stations along and behind the cube.

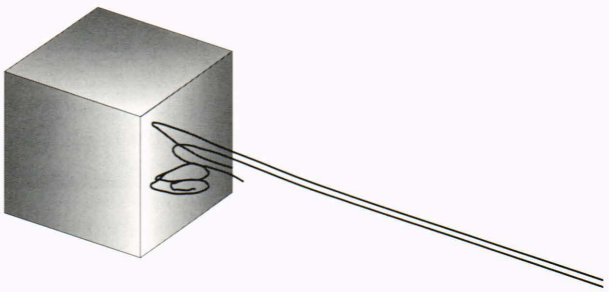

Figure 14. The motions of three particles in the wake.

port equation. The resulting closed set of equations is used to solve two relatively complex flow problems: flow around a square prism and flow around a cube. Unlike the previous applications of the present model, the nongradient terms are included in the formulation. The results are in good agreement with the experimental data. It is demonstrated that the present turbulence model can predict complex flow problems in two as well as three dimensions.

It is argued that closure models based on vorticity transport (such as the present MVC model) have a clear advantage over the ones that consider momentum transport (such as the k–ϵ model) because vorticity transport more closely follows the actual physical process of turbulence. In the future, it is proposed to carry out a more detailed analysis of the various terms involved in the closure to determine their relative contributions. An alternative derivation of the closure that will be applicable in the framework of primitive variables and its extension to compressible flows is also planned.

REFERENCES

[1] Boussinesq, J., "Théorie de l'écoulement tourbillant," in *Memoires Présentes par Divers Savants Sciences Mathematique et Physiques, Academie des Sciences, Paris*, Vol. 23, p. 46 (1877).

[2] Prandtl, L., "Über die Ausgebildete Turbulenz," *Z. Angew. Math. Mech.* **5**, 136–139 (1925).

[3] Jones, W. P., and Launder, B. E., "The Prediction of Laminarization with a Two-Equation Model of Turbulence," *Int. J. Heat Mass Transfer* **15**, 301–314 (1972).

[4] Ferziger, J. H., "Simulation of Incompressible Flows," *J. Comp. Phys.* **69**, 1–48 (1987).

[5] Lakshminarayana, B., "Turbulence Modeling for Complex Shear Flows," *AIAA J.* **24**(12), 1900–1917 (1986).

[6] Lumley, J. L., "Turbulence Modelling," *J. Appl. Mech.* **50**, 1097–1102 (1983).

[7] Lanford, O. E., "The Strange Attractor Theory of Turbulence," *Ann. Rev. Fluid Mech.* **14**, 347–364 (1982).

[8] Smyrlis, Y. S., and Papageorgiou, D. T., *Predicting Chaos for Infinite Dimensional Dynamical Systems; The Kuramoto–Sivashinsky Equation, A Case Study*, NASA Contractor Report 187531, ICASE Report No. 91-22 (1991).

[9] Turcotte, D. L., "Fractals in Fluid Mechanics," *Ann. Rev. Fluid Mech.* **20**, 5–16 (1988).

[10] Taylor, G. I., "Eddy Motion in the Atmosphere," *Phil. Trans. R. Soc.* **215**, 1–26 (1915).

[11] Taylor, G. I., "The Transport of Vorticity and Heat through Fluids in Turbulent Motion," *Proc. R. Soc.* **135A**, 685–705 (1932).

[12] Chorin, A. J., *An Analysis of Turbulent Flow with Shear*, Report FM-74-9, College of Engineering, University of California, Berkeley (1974).

[13] Bernard, P. S., "A Method for Computing Two-Dimensional Turbulent Flows," *SIAM J. Appl. Math.* **38**, 81–92 (1980).

[14] Bernard, P. S., and Berger, B. S., "A Method for Computing Three-Dimensional Turbulent Flows," *SIAM J. Appl. Math.* **42**, 453–470 (1982).

[15] Bernard, P. S. "Turbulent Vorticity Transport in Three Dimensions," *Theoret. Comp. Fluid Dynamics* **2**, 165–183 (1990).

[16] Raul, R., *A Numerical Investigation of Laminar and Turbulent Flow Past a Cube*, Ph.D. thesis, The University of Maryland (1989).

[17] Bernard, P. S., "Non-Gradient Transport Phenomena in Turbulent Shear Flows," AIAA/ASME/SIAM/APS, presented at 1st National Fluid Dynamics Congress, 25–28 Jul 1988, Cincinnati (1988).

[18] Sedov, L. I., "Decay of Isotropic Turbulent Motions of Incompressible Fluids," *Dokl. Akad. Nauk, SSSR* **42**, 116–119 (1944).

[19] Raul, R., and Bernard, P. S., "Numerical Simulation of Unsteady Forces on a Square Prism in Turbulent Flow," in *Proc. AIAA Aerosciences Meeting*, Paper AIAA-90-0582, Reno (1990).

[20] Raul, R., and Bernard, P. S., "Turbulent Cube Flow: A Numerical Investigation," in *Proc. ASME Fluids Engineering Conf., Forum on Turbulent Flows*, Toronto (1990).

[21] Hinze, J. O., *Turbulence*, 2nd Ed., McGraw–Hill, New York, p. 394 (1975).

[22] Lee, B. E., "The Effect of Turbulence on the Surface Pressure Field of a Square Prism," *J. Fluid Mech.* **69**, 263–282 (1975).

[23] Nakaguchi, H., Hashimoto, K., and Muto, S., "An Experimental Study on Aerodynamic Drag of Rectangular Cylinders," *J. Japan Soc. Aero. Space Sci.* **16**, 1 (1968).

[24] Bearman, P. W., and Trueman, D. M., "An Investigation of the Flow Around Rectangular Cylinders," *Aero. Q.* **23**, 229–237 (1972).
[25] Vickery, B. J., "Fluctuating Lift and Drag on a Long Cylinder of Square Cross-Section in a Smooth and in a Turbulent Stream," *J. Fluid Mech.* **25**, 481–494 (1966).
[26] Nakamura, Y., and Mizota, T., "Unsteady Lifts and Wakes of Oscillating Rectangular Prisms," *Ann. Soc. Civil Eng.* **101**(EM6), 855–871 (1975).
[27] Davis, R. W., and Moore, E. F., "Numerical Study of Vortex Shedding from Rectangles," *J. Fluid Mech.* **116**, 475–506 (1982).
[28] Durao, D. F. G., Heitor, M. V., and Pereira, J. C. F., "Measurements of Turbulent and Periodic Flows around a Square Cross-Section Cylinder," *Experiments in Fluids* **6**, 298–304 (1988).
[29] Okajima, A., "Strouhal Numbers of Rectangular Cylinders," *J. Fluid Mech.* **123**, 379–398 (1982).
[30] Durao, D. F. G., Heitor, M. V., and Pereira, J. C. F., "The Turbulent Flow in the Near Wake of a Squared Obstacle," in *Forum on Turbulent Flows*, Bower, W. W. (ed.), FED-Vol. 51 (1987).
[31] Nakaguchi, H., *Aerodynamic Drag Mechanisms of Bluff Bodies and Road Vehicles*, Sovran, G. S., et al. (eds.), Plenum Press, New York (1978).
[32] Anderson, H. L., *Investigation of the Forces on Bluff Bodies Near the Ground*, M.Sc. dissertation, University of London (1977).
[33] Hoerner, S. F., *Fluid Dynamic Drag*, Sec. 3, published by author, Brick Town, N.J. (1965).
[34] Raul, R., Bernard, P. S., and Buckley, F. T., "An Application of the Vorticity–Vector Potential Method to Laminar Cube Flow," *Int. J. Numer. Meth. Fluids* **10**, 875–888 (1990).
[35] Ghia, U., and Davis, T., "Navier–Stokes Solutions for Flow Past a Class of Two Dimensional Semi-Infinite Bodies," *AIAA J.* **12**, 1659–1665 (1974).
[36] Lane, J. C., and Loehrke, R. I., "Leading Edge Separation from a Blunt Plate at Low Reynolds Numbers," in *Momentum and Heat Transfer Processes in Recirculating Flows*, ASME publication HTD, Vol. 13, pp. 45–48 (1980).

THE AUTHOR

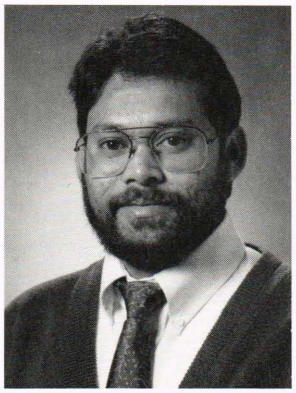

ROBIN RAUL received his B.S. degree in aerospace engineering from the Indian Institute of Technology, Kharagpur, in 1980 and his M.S. degree in aerospace engineering from the Indian Institute of Science, Bangalore, in 1982. He has also studied at The University of Maryland, where he received his Ph.D. degree in mechanical engineering in 1989. Dr. Raul has been conducting research in computational fluid dynamics at APL's Milton S. Eisenhower Research Center as a postdoctoral research associate.